Lecture Notes in Electrical Engineering 1015

Jian Dong
Long Zhang *Editors*

Proceedings of the International Conference on Internet of Things, Communication and Intelligent Technology

Springer

Lecture Notes in Electrical Engineering

Volume 1015

The book series *Lecture Notes in Electrical Engineering* (LNEE) publishes the latest developments in Electrical Engineering—quickly, informally and in high quality. While original research reported in proceedings and monographs has traditionally formed the core of LNEE, we also encourage authors to submit books devoted to supporting student education and professional training in the various fields and applications areas of electrical engineering. The series cover classical and emerging topics concerning:

- Communication Engineering, Information Theory and Networks
- Electronics Engineering and Microelectronics
- Signal, Image and Speech Processing
- Wireless and Mobile Communication
- Circuits and Systems
- Energy Systems, Power Electronics and Electrical Machines
- Electro-optical Engineering
- Instrumentation Engineering
- Avionics Engineering
- Control Systems
- Internet-of-Things and Cybersecurity
- Biomedical Devices, MEMS and NEMS

For general information about this book series, comments or suggestions, please contact leontina.dicecco@springer.com.

To submit a proposal or request further information, please contact the Publishing Editor in your country:

China

Jasmine Dou, Editor (jasmine.dou@springer.com)

India, Japan, Rest of Asia

Swati Meherishi, Editorial Director (Swati.Meherishi@springer.com)

Southeast Asia, Australia, New Zealand

Ramesh Nath Premnath, Editor (ramesh.premnath@springernature.com)

USA, Canada

Michael Luby, Senior Editor (michael.luby@springer.com)

All other Countries

Leontina Di Cecco, Senior Editor (leontina.dicecco@springer.com)

**** This series is indexed by EI Compendex and Scopus databases. ****

Jian Dong · Long Zhang
Editors

Proceedings of the International Conference on Internet of Things, Communication and Intelligent Technology

Springer

Editors
Jian Dong
Central South University
Changsha, Hunan, China

Long Zhang
School of Information Engineering
Shenzhen University
Shenzhen, Guangdong, China

ISSN 1876-1100 ISSN 1876-1119 (electronic)
Lecture Notes in Electrical Engineering
ISBN 978-981-99-0415-0 ISBN 978-981-99-0416-7 (eBook)
https://doi.org/10.1007/978-981-99-0416-7

This Springer imprint is published by the registered company Springer Nature Singapore Pte Ltd.
The registered company address is: 152 Beach Road, #21-01/04 Gateway East, Singapore 189721, Singapore

Preface

The International Conference on Internet of Things, Communication and Intelligent Technology (IoTCIT 2022) was co-organized by Central South University, China University of Mining and Technology, Hunan University and Hunan International Economics University in Changsha from August 22 to 24, 2022. As the Internet of things, communication and intelligent technology and other high-tech fields skyrocket both domestically and internationally, scientific researchers have confronted with many challenges posed by the complexity as well as the high degree interdisciplinarity. Therefore, IoTCIT 2022 was organized with a motivation to provide a platform for scholars working in related fields to showcase their research results, creating a strong community which thrives on the frontier of technology.

The conference received a positive response from the research community for its call for papers. We received a large number of submissions, which were checked for plagiarism and, if they passed the check, sent for single-blind peer review. The experts from academia were assigned as reviewers. And eighty submissions with quality and originality of work were accepted, which are divided into three parts: Internet of things, communication and intelligent technology. The accepted papers are from a broad spectrum of fields like wireless communication, signal and image processing, smart grid communication, wireless and mobile networks, information system modeling and simulation, Internet of things and big data, next generation network and many more. The sessions were interactive and brainstorming. Authors of accepted papers in the related field had participated in the conference and made oral presentations.

We would like to take this opportunity to express our deep sense of gratitude toward our committee members for the encouragement and support. Besides, we put on record our sincere thanks to our keynote speakers, sponsors, reviewers and guest editors.

Thanks are due to our authors and participants from Chinese Academy of Sciences, University of Tabriz, Iran University of Science and Technology, Sun Yat-sen University, Purdue University, University of Electronic Science and Technology of China, etc. And the tireless efforts and meticulous planning by the organizing team to make this event successful deserve special appreciation. Last but not least, we would also like to acknowledge the cooperation and support of Springer.

Changsha, China Jian Dong
Shenzhen, China Long Zhang

Introduction

The book wraps up the analytics and research portion with the application of IoT, communication and intelligent technology, presenting selected papers from the IoTCIT 2022. The papers include contributions from researchers and academics on topics in the field of Internet of things, communication and intelligent technology, which demonstrates interdisciplinary and convergent development. The proceedings will serve as a useful reference material for academics, researchers and most importantly, the student community.

Contents

Intelligent Technology

Internet of Things

The Real-Time LOS Calibration Method by Using MCP for Linear Array Whiskbroom Optical Sensor

Jun Chen[1], Jianpeng Fan[1](✉), Hui Han[2], Chen Ma[3], and Qing Zheng[4]

[1] College of Electronic Science, National University of Defense Technology, Changsha, Hunan 410073, P. R. China
jpfan@nudt.edu.cn
[2] Technical Service Center for Vocational Education, National University of Defense Technology, Changsha, Hunan 410073, P. R. China
[3] Troops 32035 PLA, Xi'an, Shanxi 71000, P. R. China
[4] Department of Military Representative Bureau of Aerospace Systems, Beijing 10000, China

Abstract. The space based infrared surveillance system (SBIRS) is a successful application of optical system which includes two different kinds of primary payloads (scanning and staring sensors). The precision of sensor's line of sight (LOS) can directly determine the precision of targets tracking and location, the timeliness of large size optical image processing even can influence the efficiency of the SBIRS. Based on researching the imaging model and characteristics of scanning sensor, this paper proposes the real-time LOS calibration methods using multi-type control points (MCPs) for improving the precision of scanning sensor's LOS. The influential factors of LOS error are equivalent to LOS attitude angles, and the theoretical model of LOS attitude angles has been used in the proposed method. By establishing the observation equation of MCPs (ground control points and star control points) and the state transition equation of LOS attitude angles, the real time high precision estimation of LOS attitude angles can be achieved for using the extend Kalman filter (EKF). The experiment results indicate that the proposed method has a high precision and a better smooth performance compared with the least squares method. And, the proposed method can also meet the requirement timeliness of for target tracking mission in SBIRS.

Keywords: SBIRS · Optical image processing · MCPs · LOS attitude angles estimation · EKF

1 Introduction

At present, the space based infrared surveillance system (SBIRS) and warning radar make up the whole missile defense system [1, 2]. Different from the warning radar, the SBIRS has many advantages owning to observation geometry. It finds the missile in the boost phase, has a wide field of view (FOV) and detects the targets outside the radar coverage area, gives the estimations of the launch point and impact point [3]. The

J. Dong and L. Zhang (Eds.): IoTCIT 2022, LNEE 1015, pp. 3–15, 2023.
https://doi.org/10.1007/978-981-99-0416-7_1

scanning sensor of SBIRS is a wide linear array whiskbroom camera, and the most important mission of scanning sensor is to find the potential targets with its wide FOV as soon as possible. Meanwhile, the timeliness and precision of the calibration method is more difficult problem for scanning sensor [4, 5]. The calibration methods of remote sensing image processing mainly include polynomial method, rational function method and collinear equation method [6–8]. However, these conventional methods do not take the subsequent changes of sensor bias into account, and they are off-line processing without real-time update. For the scanning sensor, the imaging parameters (satellite orbit, satellite attitude, and so on) are changing with each line period. Hence, the conventional methods cannot achieve the desired performance. In [8], Andy Wu proposed an LOS attitude determination and calibration method for SBIRS-high payload. In [3], Yong-Hong XUE introduced a novel target LOS calibration method by using ground control points (GCPs) for IR scanning sensor. In [5] Thomas M. Clemons put forward a bias correction technique through utilizing stellar observations for space-based EO sensor during tracking of a target.

Based on researching the imaging model and characteristics of the scanning sensor, this paper analyzes the influential factors (including the thermal distortion error, assembling error, and so on) of sensor's LOS and equivalents these factors to the LOS attitude angles. By establishing the observation equation of multi-type control points (MCPs) and the state transition equation of LOS attitude angles, the high precision estimation of LOS attitude angles can be achieved by using the filter method (extend Kalman filter, EKF). The details of the proposed methods for scanning sensor of SBIRS are given in the following.

2 LOS Calibration Model

2.1 Rigorous Imaging Model

The scanning sensor is typical linear array whiskbroom sensor. Its wide FOV is covered by the linear array detector combination of mechanical whiskbroom. The essence of imaging process is projecting the point on the surface (such as GCPs) of the earth in earth centered fix (ECF) coordinate system or the point (such as star) in earth centered inertial (ECI) coordinate system to the focal plane [3, 9], as shown in Fig. 1.

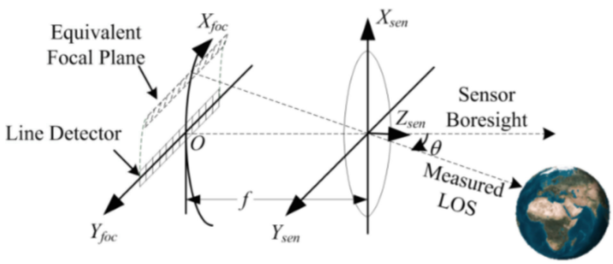

Fig. 1. The simple structure diagram of scanning sensor.

The imaging process can be described by a series of coordinate transformations. The influences of these undistinguished errors in the imaging process (thermal distortion error, optical distortion error, assembling error, orbital elements error, attitude error, etc.) are equivalent to the influences of LOS attitude angles. The LOS calibration model for scanning sensor is expressed as follow [10–13].

$$\begin{bmatrix} X - X_F \\ Y - Y_F \\ Z - Z_F \end{bmatrix}_{ECF} = m * \mathbf{R}_{Eq}(\Delta\alpha, \Delta\beta, \Delta\theta) * \mathbf{R}_{ECI}^{ECF} * \mathbf{R}_{orb}^{ECI}(\theta_\Omega, \theta_i, \theta_\omega) * \mathbf{R}_{orb}^{body}(\varphi, \varepsilon, \psi) * \mathbf{R}_{body}^{sen}(\phi_X, \phi_Y, \phi_Z) * \mathbf{M}_{mir}(\theta_0, \theta_c) * \begin{bmatrix} 0 \\ y \\ -f \end{bmatrix} \tag{1}$$

where, (X, Y, Z) represents the projective position in ECF, (X_F, Y_F, Z_F) represents satellite position in ECF, y represents the image column position in focal plane coordinate system, f represents the focal length, m represents a scale factor. $\Delta\alpha$, $\Delta\beta$, $\Delta\theta$ are the equivalent LOS attitude angles, $\mathbf{R}_{Eq}(\Delta\alpha, \Delta\beta, \Delta\theta)$ is the equivalent rotation matrix. $\mathbf{R}_{ECI}^{ECF}$ denotes the rotation from ECI to ECF; $\theta_\Omega, \theta_i, \theta_\omega$ represent the orbital elements of satellite, $\mathbf{R}_{orb}^{ECI}$ denotes the orbital elements that give the rotation from satellite orbit coordinate system to ECI; φ, ε, ψ represent the Euler angles of satellite attitude, $\mathbf{R}_{orb}^{body}$ denotes the satellite attitude angles that give the rotation from satellite body coordinate system to satellite orbit coordinate system; ϕ_X, ϕ_Y, ϕ_Z represent the assembling angles of sensor, $\mathbf{R}_{body}^{sen}$ denotes the assembling angles that give the rotation from sensor coordinate system to satellite body coordinate system; θ_0, θ_c represent the sensor pointing angles, $\mathbf{M}_{mir}$ denotes the sensor pointing angles that give the rotation from pointing coordinate system to sensor coordinate system.

Hence, the proposed method only needs to estimate the LOS attitude angles for completing the real-time LOS calibration mission.

2.2 LOS Attitude Angles Model

All on-orbit satellites suffer from a cyclical cooling and heating space environment owing to the circular orbit around the earth. The thermal distortion error which results from the satellite enters and comes out of earth caused solar eclipse is the biggest error in the imaging process [14]. This error has the same period with the satellite orbit and is presenting in three axes. The optical distortion error and the assembling error which caused by satellite launching and injecting are usually unchanged or changing slowly [5]. These errors are the main factors to influence the sensor LOS. From what has been discussed about the characteristics of the main factors, each axis LOS attitude angle is expressed by a constant bias and a cosine component as follow [5, 14].

$$\begin{cases} \alpha(t) = \varsigma_\alpha + A_\alpha \cos(\omega_\alpha t + \zeta_\alpha) \\ \beta(t) = \varsigma_\beta + A_\beta \cos(\omega_\beta t + \zeta_\beta) \\ \theta(t) = \varsigma_\theta + A_\theta \cos(\omega_\theta t + \zeta_\theta) \end{cases} \tag{2}$$

where, $\varsigma_\alpha, \varsigma_\beta, \varsigma_\theta$ are the constant components, $A_\alpha, A_\beta, A_\theta$ are the amplitudes of the cosine component, $\omega_\alpha, \omega_\beta, \omega_\theta$ are the frequencies of the cosine component, and $\zeta_\alpha, \zeta_\beta, \zeta_\theta$ are the phases of the cosine component.

3 Technical Approach

3.1 Determine the Background Observations

The scanning sensor of SBIRS can observe both GCPs and star control points (SCPs) with the high extracting precision in observation background due to the orbit motion of high ellipse orbit. Meanwhile, the same GCP can be observed in sequence image with different satellite positions and pointing angles because of the orbit motion and mechanical whiskbroom. And this can hamper the extracting precision of GCPs. In this paper, the proposed method uses the multi-type control points (MCPs, GCPs and SCPs) to calibrate the scanning sensor LOS of SBIRS.

Determine the Background Observations of SCPs. Whether there are enough stars in the FOV of scanning sensor is the most important issue what we should pay attention to. The Wide-field Infrared Survey Explorer (WISE) preliminary data which released by the infrared astronomical satellite in 2011 is used in this study. Refer to [8], the scanning sensor of SBIRS can detect nearly 1551 IR stars in one orbit period. Figure 2(a) shows the distribution of observed stars in the sky which are represented by the red dots; the green dots represent the stars in the FOV of sensor which are sheltered by the earth; the blue dots represent the stars outside the FOV of sensor. Figure 2(b) shows the number of observed star with the time-varying.

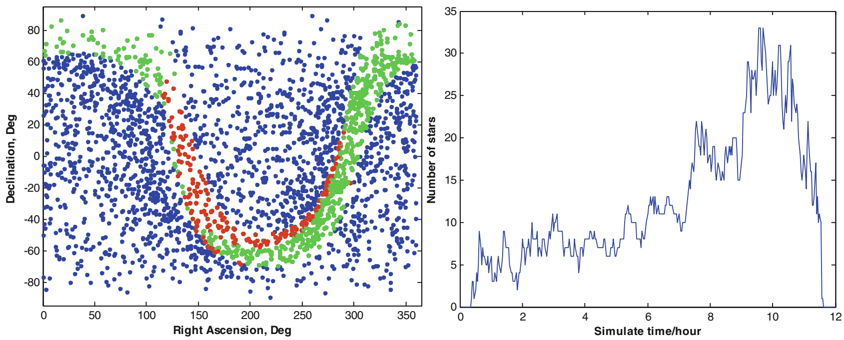

Fig. 2. (**a**) The distribution of observed stars in the sky, (**b**) the number of observed stars with the time-varying

How to rapidly extract and match the stars is the next important issue. In this paper, the centroid weight method is used to high precision extract the image positions of stars. From the Fig. 2b, only a few numbers of stars can be observed by the scanning sensor in one frame period. It is a time-consuming work that searches all WISE data to match the candidate stars in the sensor FOV. So, the WISE data is divided into some small sub-catalog in advance for the rapidly star matching, and then, the sensor LOS has been calculated to decide which sub-catalog should be used in star matching [9].

Determine the Background Observations of GCPs. For remote sensing image, the template images of GCPs are usually generated before GCPs extraction and matching and used for a long time [15]. The scanning sensor is used to meet the mission demand of high frequency monitoring coverage area. Due to the orbit motion and mechanical whiskbroom, the same GCP can be observed in sequence image with different satellite positions and pointing angles. While, the different pointing angles can lead to the different image shapes for one GCP. If we still use the fixed template image for GCPs extraction and matching, it could deteriorate the accuracy of GCPs extraction and matching. The simulation images of Taiwan Island (E 121.9°, N 24.7°) with different pointing angles are shown in Fig. 3(a), b.

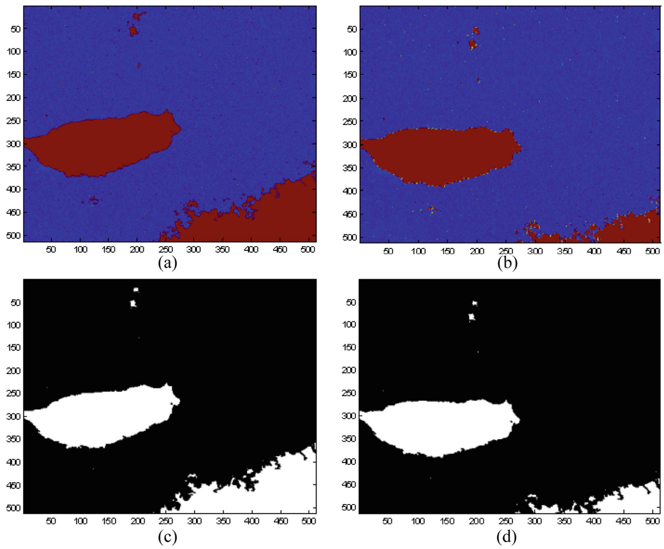

Fig. 3. (**a**–**b**) The images of Taiwan Island with different pointing angles, (**c**–**d**) the real-time generation of GCPs templates

Based on these characteristics of scanning sensor, we use the imaging model and imaging parameters to generate the template images of GCPs in real time for eliminating the influence of the pointing angle. The simulation data comes from Shuttle Radar Topography Mission (SRTM). The details of generation GCPs template are presented in [16]. The real-time template images of Taiwan Island with different pointing angles are shown in Fig. 3(c–d).

3.2 The Procedure of Proposed Method

The real-time LOS calibration method using MCPs consists of four primary steps: (1) determine the background MCPs observations; (2) obtain the LOS attitude angles measurements; (3) estimate the LOS attitude angles; (4) calibrate the target LOS. The procedure of proposed method is shown in Fig. 4.

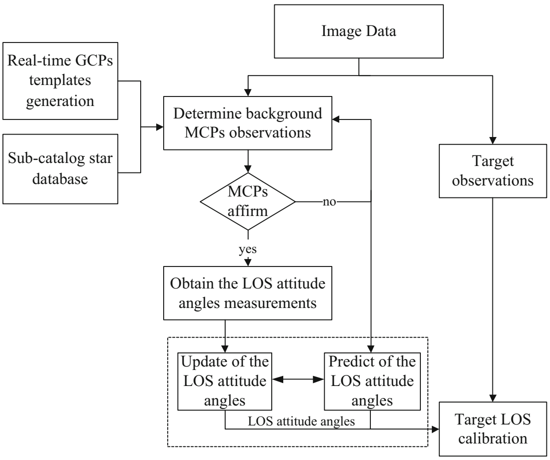

Fig. 4. The flowchart of proposed method

3.3 Derivation of EKF

State Variables and State Transition Equation. The desirable state variables should be selected for exactly estimating the LOS attitude angles. And the state transition equation can be established based on the changing rule of the state variables. According to the Eq. (1), we need to obtain the estimation of the LOS attitude angle for each axis. Hence, three separate EKFs with the state vector modeled as the magnitude of LOS attitude angles, the changing rate of LOS attitude angles, and the frequency of the cosine component in LOS attitude angles for each axis, such that:

$$\begin{cases} \alpha_k = \left[\alpha_k \ \dot{\alpha}_k \ \omega_{\alpha,k}\right]^T \\ \beta_k = \left[\beta_k \ \dot{\beta}_k \ \omega_{\beta,k}\right]^T \\ \theta_k = \left[\theta_k \ \dot{\theta}_k \ \omega_{\theta,k}\right]^T \end{cases} \tag{3}$$

According to Eq. (2), we take the one-dimensional LOS attitude angle as an example. The first-order and two-order derivatives of the one-dimensional LOS attitude angle can be expressed as follow.

$$\dot{\alpha}(t) = -A_\alpha \omega_\alpha \sin(\omega_\alpha t + \zeta_\alpha) \tag{4}$$

And

$$\ddot{\alpha}(t) = -A_\alpha \omega_\alpha^2 \cos(\omega_\alpha t + \zeta_\alpha) \tag{5}$$

For the case of $\varsigma_\alpha \approx 0$, the Eq. (5) can be simplified as follow.

$$\ddot{\alpha}(t) \approx -\alpha(t)\omega_\alpha^2 \tag{6}$$

Account for some random frequency variations, the process noise model $\dot{\omega}_\alpha(t) = \mu_\alpha(t)$ has been applied in here, $\mu_\alpha(t)$ is a spectral density of Θ_{ω_α}. Therefore, the state transition equation can be described as follow [10].

$$\begin{bmatrix} \dot{\alpha} \\ \ddot{\alpha} \\ \dot{\omega}_\alpha \end{bmatrix} = \begin{bmatrix} 0 & 1 & 0 \\ -\omega_\alpha^2 & 0 & 0 \\ 0 & 0 & 0 \end{bmatrix} \begin{bmatrix} \alpha \\ \dot{\alpha} \\ \omega_\alpha \end{bmatrix} + \begin{bmatrix} 0 \\ 0 \\ \mu_\alpha \end{bmatrix} \tag{7}$$

The discrete state transition equation can be expressed as follow by the linearization and discretization of the nonlinear continuous system.

$$X_k = \Phi X_{k-1} + \upsilon_{k-1} \tag{8}$$

where, $X_k = [\alpha_k; \beta_k; \theta_k]$ is the discrete state vector of sampling time k. $\Phi = diag[\Phi_\alpha, \Phi_\beta, \Phi_\theta]$ is the fundamental matrix. $\upsilon_{k-1} = \left[\upsilon_\alpha; \upsilon_\beta; \upsilon_\theta\right]$ is the corresponding process noise with the covariance matrix $\mathbf{Q}_{k-1} = diag[Q_\alpha, Q_\beta, Q_\theta]$, $\upsilon_\alpha = [0, 0, \mu_\alpha]^T$, $\upsilon_\beta = \left[0, 0, \mu_\beta\right]^T$, $\upsilon_\theta = [0, 0, \mu_\theta]^T$. $\Phi_\alpha, \Phi_\beta, \Phi_\theta$ and $Q_\alpha, Q_\beta, Q_\theta$ have the same construct respectively, so we take Φ_α and Q_α as the examples for describing their constructs [19].

$$\Phi_\alpha \approx I + \frac{\partial f(\overline{\alpha})}{\partial \overline{\alpha}} T_s = \begin{bmatrix} 1 & T_s & 0 \\ -\hat{\omega}_{\alpha,k-1}^2 T_s & 1 & -2\hat{\omega}_{\alpha,k-1}\hat{\alpha}_{k-1}T_s \\ 0 & 0 & 1 \end{bmatrix} \tag{9}$$

where, T_s is the time step interval of the measurement. It is the line sampling time of scanning sensor.

$$\begin{aligned} Q_\alpha = E\{\upsilon_\alpha \upsilon_\alpha'\} &= \int_0^{T_s} \Phi_\alpha(\tau)\Omega\Phi_\alpha^T(\tau)d\tau \\ &= \begin{bmatrix} 0 & 0 & 0 \\ 0 & \frac{4}{3}\hat{\omega}_{\alpha,k-1}^2\hat{\alpha}_{k-1}^2 T_s^3 \Theta_{\omega_\alpha} & -\hat{\omega}_{\alpha,k-1}\hat{\alpha}_{k-1}T_s^2\Theta_{\omega_\alpha} \\ 0 & -\hat{\omega}_{\alpha,k-1}\hat{\alpha}_{k-1}T_s^2\Theta_{\omega_\alpha} & T_s\Theta_{\omega_\alpha} \end{bmatrix} \end{aligned} \tag{10}$$

where, $\Phi_\alpha^T(\tau)$ is the transposed matrix of $\Phi_\alpha(\tau)$.

3.3.1 Observation Equation

The observation equation of SCPs. The SCPs residuals are defined as the differences between the estimated right ascension (RA) and declination (DEC) of SCPs and the true RA and DEC of SCPs [9]. The true RA and DEC angles $\alpha'_{ECI}, \beta'_{ECI}$ in ECI can be obtained after the SCPs matching. The estimated RA and DEC angles $\hat{\alpha}'_{ECI}, \hat{\beta}'_{ECI}$ in ECI can be calculated according to the Eq. (10) by using the imaging parameters and the real image positions of SCPs. Hence, the SCPs residuals $\Delta\alpha'$, $\Delta\beta'$ are calculated as follows.

$$\begin{aligned} \Delta\alpha' &= \alpha'_{ECI} - \hat{\alpha}'_{ECI} \\ \Delta\beta' &= \beta'_{ECI} - \hat{\beta}'_{ECI} \end{aligned} \tag{11}$$

The relationship between the SCPs residuals and the LOS attitude angles can be expressed as follow.

$$\begin{cases} \alpha = \cos^{-1}(\cos\Delta\alpha' \cos\Delta\beta') \\ \beta = \cos^{-1}(\sin\Delta\alpha' \cos\Delta\beta') \\ \theta = \cos^{-1}(\sin\Delta\beta') \end{cases} \tag{12}$$

The observation equation of GCPs. The GCPs residuals are defined as the differences between the estimated longitude and latitude of GCPs and the true longitude and latitude of GCPs in ECF. Once the extraction and matching of GCPs have been completed, the estimated longitude and latitude of GCPs $\hat{B}_{ECF}$, $\hat{L}_{ECF}$ can be computed according to the Eq. (10) by using the image parameters and the real image positions of GCPs. Hence, the GCPs residuals $\Delta\alpha'$, $\Delta\beta'$ are calculated as follow. And the relationship between the GCPs residuals and the LOS attitude angles can be expressed as follow.

$$\begin{aligned} \Delta\alpha' &= B_{ECF} - \hat{B}_{ECF} \\ \Delta\beta' &= L_{ECF} - \hat{L}_{ECF} \end{aligned} \tag{13}$$

According to the Eq. (12), we only obtain the measurement of magnitude of LOS attitude angles in each control point observation. The measurement variables are defined as follow:

$$\begin{cases} Z_{\alpha,k} = \begin{bmatrix} \alpha_k & 0 & 0 \end{bmatrix}^T \\ Z_{\beta,k} = \begin{bmatrix} \beta_k & 0 & 0 \end{bmatrix}^T \\ Z_{\theta,k} = \begin{bmatrix} \theta_k & 0 & 0 \end{bmatrix}^T \end{cases} \tag{14}$$

The measurement vector of sampling time k is defined as $\mathbf{Z}_k = \left[Z_{\alpha,k}; Z_{\alpha,k}; Z_{\theta,k}\right]$. The observation equation is used to describe the relationship between the discrete state vector and measurement vector. So, the observation equation of two kinds of control points can be represented as follow:

$$\mathbf{Z}_k = \mathbf{H}_k \mathbf{X}_k + v_k \tag{15}$$

where, $\mathbf{X}_k$ is the discrete state vector of sampling time k. $\mathbf{H}_k = diag\left[\mathbf{H}_\alpha; \mathbf{H}_\beta; \mathbf{H}_\theta\right]$ is the observation matrix. v_k is the measurement noise, $E\{v_k\} = 0$, $E\{v_k^2\} = \mathbf{R}_k \delta_{ki}$, and the $\mathbf{R}_k = \sigma_v^2$ is the measurement noise variance.

The steps of EKF. The main steps of EKF are listed as follows [17].

(a) Propagate the covariance matrix $\mathbf{P}_{k/k-1}$ and the estimated state vector $\hat{\boldsymbol{X}}_{k/k-1}$.

$$\mathbf{P}_{k/k-1} = \Phi_{k-1}\mathbf{P}_{k-1/k-1}\Phi_{k-1}^{\mathrm{T}} + \mathbf{Q}_{k-1} \tag{16}$$

$$\hat{\boldsymbol{X}}_{k/k-1} = \Phi_{k-1}\hat{\boldsymbol{X}}_{k-1/k-1} \tag{17}$$

(b) Compute the gain matrix $\mathbf{K}_k$ based on the MCPs observations.

$$\mathbf{K}_k = \mathbf{P}_{k/k-1}\mathbf{H}_k^{\mathbf{T}}(\mathbf{H}_k\mathbf{P}_{k/k-1}\mathbf{H}_k^{\mathbf{T}} + \mathbf{R}_k)^{-1} \tag{18}$$

(c) Update the covariance matrix $\mathbf{P}_{k/k}$ and the estimated state vector $\hat{\boldsymbol{X}}_{k/k}$.

$$\mathbf{P}_{k/k} = (\mathbf{I} - \mathbf{K}_k\mathbf{H}_k)\mathbf{P}_{k/k-1} \tag{19}$$

$$\hat{\boldsymbol{X}}_{k/k} = \hat{\boldsymbol{X}}_{k-1/k-1} + \mathbf{K}_k(\mathbf{Z}_k - \mathbf{H}_k\hat{\boldsymbol{X}}_{k/k-1}) \tag{20}$$

4 Experiment

To verify the superior performance of the real-time sensor LOS calibration method, we design two experiments in this paper. In the first experiment, the EKF method is compared with the least square method (LS method). The second experiment shows the high calibration precision by using the MCPs. The details of experiments are described as follow.

4.1 Method Comparison

Simulation Scene Description. There are two kinds of inputs in this experiment. The one is GCPs which are used to estimate the LOS attitude angles. The other is Random Check Points (RCPs) which are picked out randomly to accurately evaluate the performances of two methods. We randomly select 10 GCPs and 30 RCPs in each frame. The beginning time of simulation is 8 JUL 2021 15:30:00 UTCG and the ending time is 8 JUL 2021 18:30:00 UTCG. The simulation parameters are defined as follow. The satellite position error is set to 600 m in each direction, the satellite velocity error is set to 100 m/s in each direction, the satellite attitude error is set to 10″ in each axis, the sensor assembling error is set to 40″ in each axis, the sensor pointing error is set to 10″, the frame period of sensor is set to 5 s, the angle resolution of sensor is set to 60 μrad. To adequately compare the EKF method and the LS method, we have designed different testing scenes according to the Eq. (2) in this experiment, the parameters of three-dimensional LOS attitude angles are listed in Table 1.

Experiment Result. The angle between the calibrated LOS vector $\mathbf{r}_{ECI}^{cal}$ and the true LOS vector $\mathbf{r}_{ECI}^{true}$ in ECI is used as the criterion of the calibration precision and calculated as follow [3].

$$\phi = \arccos\left(\frac{\left(\mathbf{r}_{ECI}^{true}\right)^{\mathrm{T}}\mathbf{r}_{ECI}^{cal}}{\left\|\mathbf{r}_{ECI}^{true}\right\| \cdot \left\|\mathbf{r}_{ECI}^{cal}\right\|}\right) \tag{21}$$

Table 1. The parameters of different testing scenes

Scene No.	1 (μrad)	2 (μrad)	3 (μrad)	4 (μrad)	5 (μrad)
Parameters	$\varsigma = 0.00$ $A = 0.24$	$\varsigma = 0.60$ $A = 0.24$	$\varsigma = 1.20$ $A = 0.24$	$\varsigma = 1.20$ $A = 0.06$	$\varsigma = 1.20$ $A = 0.48$

The calibration results of RCPs using two methods with the first 100 s of scene 3 are shown as follow.

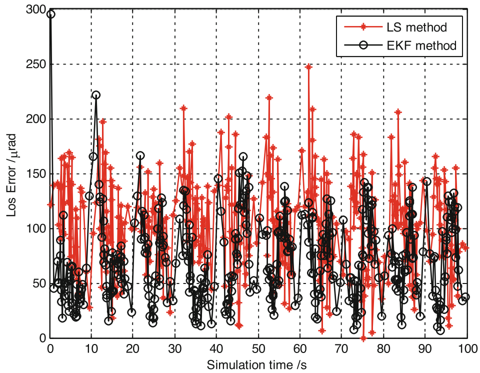

Fig. 5. The calibration results of RCPs using two different inputs

Table 2. The calibration results of two methods in different scenes

Scene No.	The EKF method		The LS method	
	Mean value (μrad)	Variance	Mean value (μrad)	Variance
1	90.83	41.33	92.08	48.92
2	91.57	40.29	91.19	49.13
3	90.73	42.18	92.33	48.51
4	89.11	39.66	90.18	46.17
5	95.35	44.74	121.65	62.36

The calibration results of two methods in different scenes are shown in Table 2. In the Fig. 5, the simulation results show that the EKF method is an effective method for calibrating the scanning sensor's LOS attitude and has a fast speed convergence in comparison with the LS method, the EKF has converged in the twentieth second. Meanwhile, the calibration results contain the wave phenomenon, this is mainly because the GCPs only distribute in the middle of the image, when the SCPs distribute in the space area, the calibration results would diverge. When the EKF method converges, it has a similar performance with the LS method in the scene 3. From the Table 2, the simulation results show that the performance of the EKF method is better than the LS method in all testing scenes. The mean of the EKF method is similar to the LS method. However, the standard deviation of the EKF method is better than the LS method, so the EKF method has the smoother and steadier performance. We find that the EKF method has the similar performance in the scene 1–3. The experiment results of scene 3–5 indicate that the performance of two methods deteriorate with the growing the amplitude of the cosine components. Nevertheless, the EKF method can obtain a preferable calibration result even in the scene 5. It is because that the model of the LOS attitude angles is used in the EKF method. The other important thing is that the EKF method can do the calibration work as soon as the target is detected, does not need to wait until the whole image is obtained and has a much better timeliness in comparison with the conventional method.

4.2 Method Verification

Simulation Scene Description. The simulation scene is same as the last one. We use the parameters of LOS attitude angles in scene 3. And, we use three sets of CPs to test the performance of the EKF method. The first set contains two kinds of CPs: GCPs and SCPs, the second set only contains SCPs, the third set only contains GCPs. It is well-known that the extracting precision of SCPs is better than the extracting precision of GCPs, even if we used the real-time templates in the GCPs extraction and matching. So, the extraction error of GCPs is 60 μrad and the extraction error of SCPs is 30 μrad in this experiment. The RCPs also have been used to accurately evaluate the performances of the proposed method in different sets. We randomly select 10 CPs and 30 RCPs in each frame for three sets.

Experiment Result. The calibration results of RCPs using three different input sets with the first 100 s of the scene are shown in Fig. 6, and the performance statistics are listed in Table 3.

In the Fig. 6, the calibrated results using the first input set has a fast speed convergence and a good smoothness compared with the calibrated results using the second or third input set. There are a lot of divergence points in the calibrated results using the second and third input sets. It is obvious that the number of divergence points in calibrated results using the second input set is more than the divergence points in calibrated results using the third input set. This is because the proportion of the space background is smaller than the earth background and the distribution of SCPs is more uneven than GCPs in the image of scanning sensor. Due to the higher extracting precision of SCPs, the convergence points in calibrated results using the second input set have a superior performance than the convergence points in calibrated results using the third input set.

From the Table 3, the mean value of the calibrated results using second input set is like the calibrated results using third input set, while the variance of the calibrated results using second input set is worse than the calibrated results using third input set. And, the first input set can obtain the most efficient performance in three sets. There are two reasons: (1) the SCPs distribute at the both ends of the scanning image, the GCPs distribute in the middle of the scanning image, so the MCPs (SCPs and GCPs)

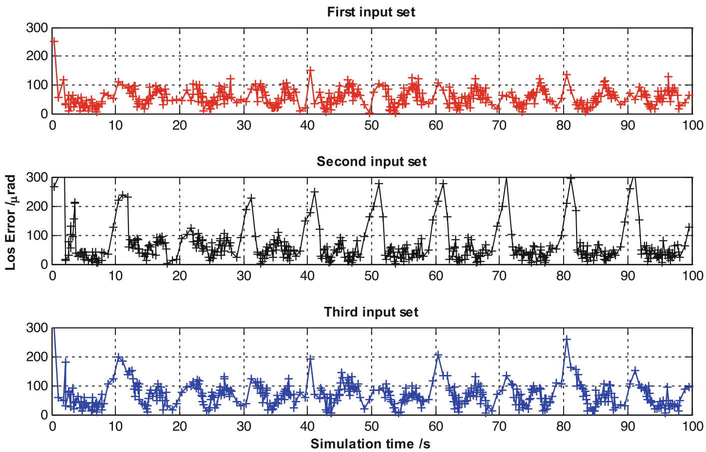

Fig. 6. The calibration results of RCPs using three different input sets

Table 3. The calibration results of three different input sets

	Mean value (μrad)	Variance
First input set	60.49	31.36
Second input set	91.33	65.82
Third input set	89.42	41.64

can distribute evenly compared with the GCPs or SCPs; (2) the extracting precision of SCPs is better than the GCPs. And, the simulation result show that the proposed method by using the MCPs can effectively improve the LOS calibration precision of scanning sensor and achieve the precision of about one pixel (the angle resolution of sensor is set to 60 μrad).

5 Conclusions

The LOS calibration of scanning sensor is a significant work in SBIRS. This paper proposes a LOS calibration method using MCPs for scanning sensor which can real-time calibrate the errors that result from thermal or dynamic effects on the system while the target is in track. The experiment results indicate that the performance of proposed method has been improved to about one pixel by using MCPs. So, the proposed method can deal with the situation of GCPs deficiency (such as cloud covered). Compared with the conventional methods (such as LS method), the most important thing is that the proposed method does not need to accumulate the CPs. Once the target is detected, the calibration work can be completed by the proposed method in real-time. And this study contributes to the high precision of target's tracking and location in SBIRS.

References

1. Andreas, N.S.: Space based infrared system (SBIRS) system of systems. In: IEEE Aerospace Conference Proceedings, pp. 429–438 (1997)
2. Slattery, J.E., Cooley, P.R.: Space-based infrared satellite system (SBIRS) requirements management. In: IEEE Aerospace Conference Proceedings (1998)
3. Xue, Y., An, W.: A novel target LOS calibration method for IR scanning sensor based on control points. In: Proceedings of SPIE, pp. 314–318 (2012)
4. Sheng, W., Xu, Y., Zhou, Y.: Analysis of LOS measurement error for space-based optical sensor. J. Astronaut. **32**, 129–135 (2011)
5. Clemons, T.M., Chang, K.C.: Sensor calibration using in-situ celestial observations to estimate bias in space-based missile tracking. IEEE Trans. AES **48**(2), 1403–1427 (2012)
6. Sun, J., Ni, L., Zhou, J.: Principle and Applications of Remote Sensing, pp. 123–137. Wuhan University Press (2009)
7. Poli, D., Toutin, T.: Review of developments in geometric modeling for high resolution satellite pushbroom sensors. Photogramm. Rec. **27**, 58–73 (2012)
8. Wu, A.: SBIRS high payload LOS attitude determination and calibration. In: IEEE Aerospace Conference Proceedings, pp. 243–253 (1998)
9. Chen, J., An, W., Deng, X., Yang, J., Xu, Z.: Space based infrared scanning sensor LOS determination and calibration using star observation. In: Proceedings of SPIE (2015)
10. Chen, Y.F., Xie, Z., Qiu, Z., Zhang, Q., Hu, Z.: Calibration and validation of ZY-3 optical sensors. IEEE Trans. Geosci. Remote Sen. **53**, 4616–4626 (2015)
11. Jiang, Y., Zhang, G., Tang, X., Li, D., Huang, W., Pan, H.: Geometric calibration and accuracy assessment of ZiYuan-3 multispectral images. IEEE Trans. Geosci. Remote Sen. **52**(7), 4161–4172 (2014)
12. Li, L., Zhang, G., Jiang, Y., Shen, X.: An improved on-orbit relative radiometric calibration method for agile high-resolution optical remote-sensing satellites with sensor geometric distortion. IEEE Trans. Geosci. Remote Sen. **60**, 1–15 (2022)
13. Wang, M., Cheng, Y., Tian, Y., He, L., Wang, Y.: A new on-orbit geometric self-calibration approach for the high-resolution geostationary optical satellite GaoFen4. IEEE J. Sel. Top. Appl. Earth Observ. Remote Sens. **11**(5), 1670–1683 (2018)
14. Kistosturian, H.G.: On-orbit calibration of satellite antenna-pointing errors. IEEE Trans. AES **26**, 88–1121 (1990)
15. Eppler, W.G., Paglieroni, D.W.: GOES landmark positioning system. In: Proceedings of SPIE, pp. 789–804 (1996)
16. Wang, P., Deng, X., Zhang, X.: A new method to obtain ground control points based on SRTM data. In: 5th International Symposium on Photoelectronic Detection and Imaging (2013)
17. Zarchan, P., Usoff, H.M.: Fundamentals of Kalman Filtering: A Practical Approach, 3rd edn., pp. 417–420. AIAA, Reston, VA (2009)

Check for updates

Design and Research of Aquaculture Monitoring Equipment Based on IoTs

Haowei Fu, Yaonuan Wang, Liangdi Yao, Yilin Chen, and Youfu Jiang(✉)

School of Information Engineering, Zhejiang Ocean University, Zhoushan 316022, Zhejiang, China

jiangyoufu@zjou.edu.cn

Abstract. In this paper, a fisheries aquaculture water quality monitoring system based on the IoT is designed. The design of the system is based on the development board STM32F103 as the main controller. The system uses WIFI wireless transmission network, wireless module equipped with various monitoring sensors, real-time collection of aquaculture site water quality temperature, turbidity value and other data. The data is transmitted to the monitoring interface of the top computer to provide real-time monitoring interface for aquaculture personnel. After our system test, the water quality information of fishery aquaculture environment can be monitored, which confirms the feasibility of the system.

Keywords: Iot · Water quality monitoring · Wireless sensor network

1 Introduction

China's fishery develops rapidly, but in some traditional aquaculture, water quality monitoring mainly relies on traditional manual monitoring methods. However, manual sampling method will have a large workload, and its monitoring scope and time are also very limited, and can not accurately monitor the required water quality data information. In the current field of fishery Internet of Things, advanced Internet of Things technology is usually applied in fisheries, so as to improve the efficiency of fishery breeding. Encinas et al. [1] designed a prototype of aquaculture water quality monitoring based on wireless sensor networks, Chen and Han [2] designed a water quality monitoring in smart city: A pilot project, Shixian et al. [3] designed a water quality online monitoring system based on Internet of Things technology. In this article, the designed system using some of the fishery IoT technology, complete real-time acquisition of aquaculture water quality parameters of the information, to adapt to the modern intelligence cultivation pattern, at the same time satisfy the needs of convenience, environmental protection, high efficiency, low cost, etc. Based on the terminal sensor of the Internet of Things, a complete set of data acquisition system is combined through the WIFI wireless [4] communication module to realize the processing of water quality detection data and the control of the lower computer. Through docking with the platform, detected data can be saved to the platform for data processing, and the development from traditional manual farming to modern equipment farming [5] will help improve the survival rate of fish farming. We mainly built several modules to solve the following problems:

J. Dong and L. Zhang (Eds.): IoTCIT 2022, LNEE 1015, pp. 16–21, 2023.
https://doi.org/10.1007/978-981-99-0416-7_2